BEHAVIOR AND PREDICTION OF REINFORCED SLOPES AND WALLS

Tamotsu Matsui
Professor
Osaka University
Suita, Osaka 565, Japan

ABSTRACT

In this paper, behavior of reinforced cut slopes due to root piles and reinforced retaining walls due to geosynthetics was monitored, followed by comparing with the results of FEM prediction. Two full-scale field tests for reinforced cut slopes and two large-scale model tests for reinforced retaining walls were carried out. As the results, some important reinforcement mechanisms were elucidated through measured data and avalytical results, followed by demonstrating the availability of FEM prediction for reinforced slopes and walls.

KEYWORDS

Finite element method, field test, model test, prediction, reinforced cut slope, reinforced earth

INTRODUCTION

Various techniques of reinforced soils have recently been introduced as a cost-effective soluftion to problems such as unstable slopes and retaining walls. However, their mechanism has not well understood so far. Consequently, many laboratory element and model tests, field measurements and field tests, and limit equilibrium analyses and fimite element simulations have been performed.

In this paper, behavior of reinforced cut slopes due to root piles and reinforced retaining walls due to geosynthetics was monitored, followed by comparing with the results of FEM prediction. As for reinforced cut slopes, two full-scale field tests were carried out, being incorporated with road improvement projects in Osaka, Japan. As for reinforced retaining walls, two large-scale model tests were carried out, to provide data for a prediction symposium on the geotextile-reinforced retaining wall behavior and to elucidate the mechanism of reinforced wall. Through these measured data and analytical results of reinforced slopes and walls, their reinforcement mechanism is discussed, followed by demonstrating the availability of the FEM prediction.

OUTLINE OF TEST SITES ON REINFORCED CUT SLOPES AND ROOT PILE METHOD

The two field test sites, Kashiwara and Nose, are located at mountainous region in the suburbs of Osaka, as shown in Fig. 1. In Kashiwara test site, the existed road is at the mid-level of slope with the elevation of about 300 m above sea level. The slope consists dominantly of an inclined gneiss-granite soft rock stratum overburdened by a completely decomposed granite residual soil layer of several meters with a dip of 20° - 35°. In the nearby area, a slope failure happened previously during the cutting in the road widening works. In order to ensure the long term slope stability of the cut slope and the safety of the cutting during construction, in-situ slope stabilization by root piles was used in some part of cutting in the road widening project. The proposed plan and section of the reinforced cut slope are shown in Figs. 2 and 3, respectively.

In Nose test site, the existed road is at the mid-level of slope with the elevation of about 600 m above sea level. The slope consists of sand stone with inclined joints of about 40°. In the nearby area, a slope failure happened previously during the cutting in the road widening works. As many notable cracks were observed in the existing concrete retaining wall at the test site, slope remedial works were planned. In-situ slope stabilazation by root piles was employed to protect this slope against a slip failure. The proposed plan and section of the reinforced cut slope are shown in Figs. 4 and 5, respectively.

As for applied root pile method, in order to install reinforcements of root piles, the excavation of slope is carried out by steps with a certain pitch, for example 2.5 m. After the completion of each step of excavation, drilling hole of diameter of 116 m is formed by a rotary drill. The reinforcement of root pile is a small steel pipe with 36 mm in diameter and 6 mm in

thickness. The root pile is formed by grouting the steel pipe with expansive mortar. In order to increase the friction between the mortar and the soil, special rings are fixed on the steel pipe at 500 mm interval. The head of root pile is fixed with a bearing plate and a nut, as shown in Fig. 6. The surface of the cutting is protected by 30 mm thick mortar of shotcrete with a steel mesh.

KASHIWARA CASE – COMPARISON OF SURCHARGE AND EXCAVATION EFFECTS

Field Test and Procedure

In order to compare surcharge and excavation effects on a reinforced cut slope, field loading and excavation tests were performed (Matsui, San, Amano and Otani, 1988) . Fig. 7 shows the section and the elevation of the reinforced slope for the field test. The gradient of the slope cutting is 1 : 0.3. The soil profile at the borehole location is shown in Fig. 8. The thichness of the decomposed granite layer is about 7 m from the top of slope. The physical properties and the result of LLT for the decomposed granite are given in Tables 1 and 2. The cohesion and the internal friction angle of the residual soil obtaining from the drained triaxial tests are 27 kPa and 45°, while those from the back analysis of the previous landslide are 10 kPa and 19°, respectively. The difference between them may be caused by the relic joint in the residual soil. The shear strength parameters obtaind from the triaxial tests possibly are the intact strength of the residual soil, while those from the back calculation could be the avarage of the strength of the residual soil with relic joints at the field condition.

The loading test was carried our by piling up the sandbags on the top of slope, in order to apply a uniformly distributed load. The sandbags were placed at a controlled loading speed of 5.9 kPa/h, and the maximum load was 50 kPa. The loading curve

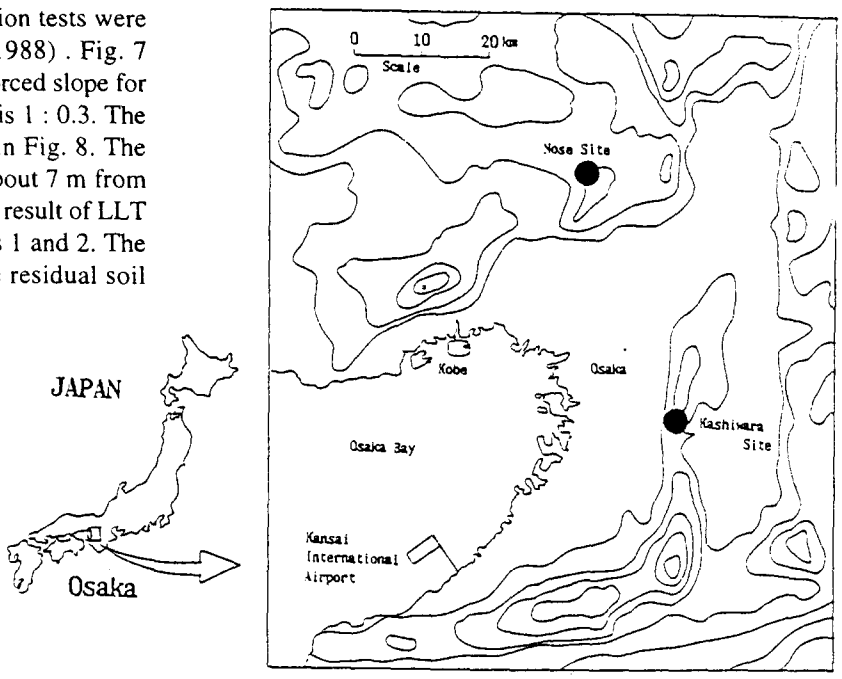

Fig. 1 Location of two field test sites

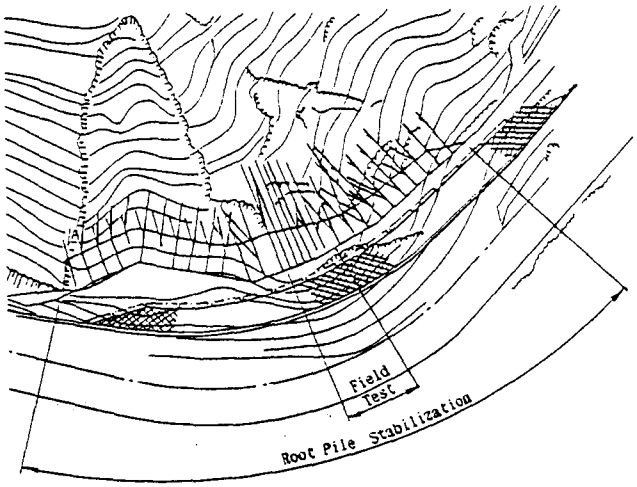

Fig. 2 Plan of reinforced slope (Kashiwara site)

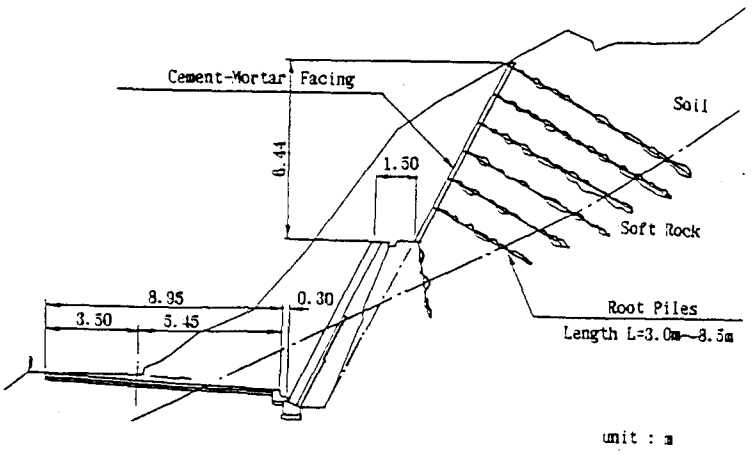

Fig. 3 Section of reinforced slope (Kashiwara site)

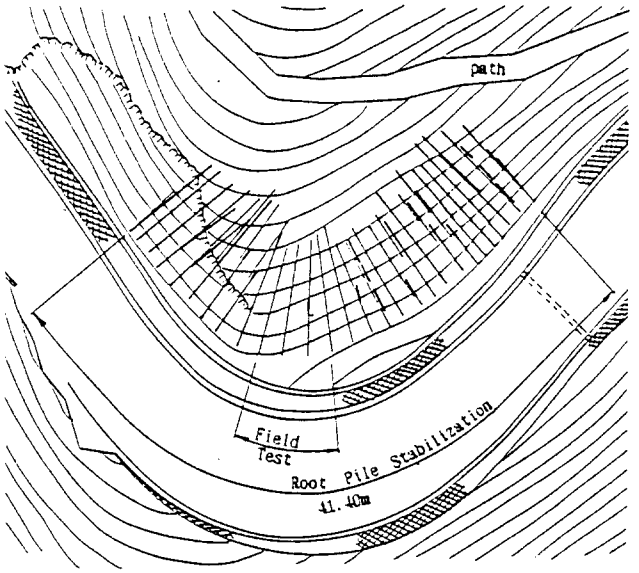

Fig. 4 Plan of reinforced slope (Nose site)

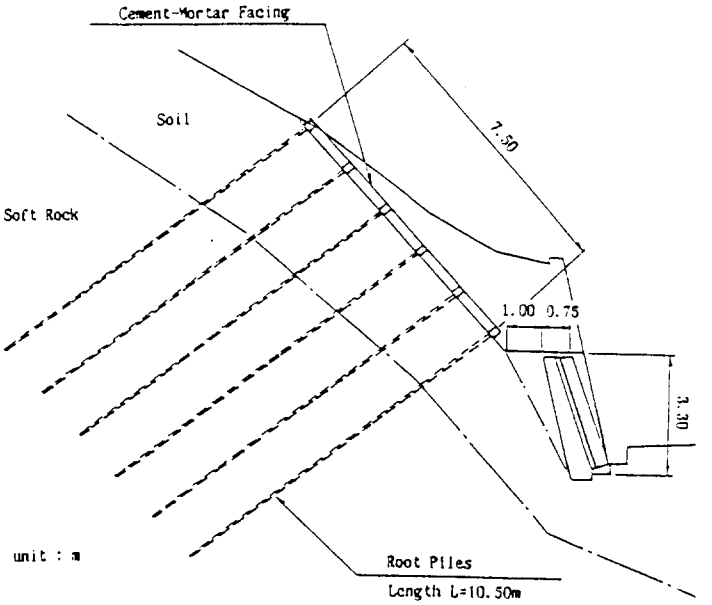

Fig. 5 Section of reinforced slope (Nose site)

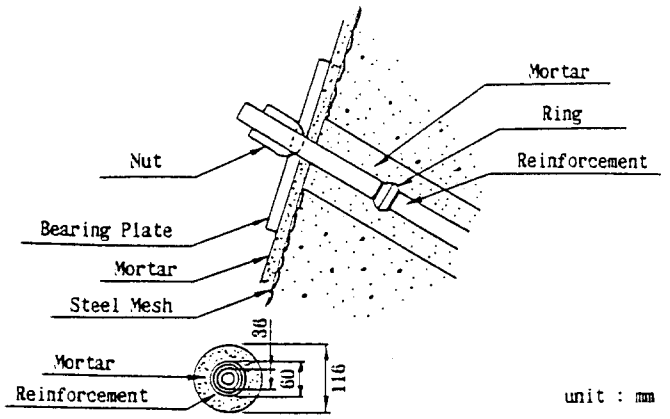

Fig. 6 Section of root pile

is shown in Fig. 9. For the purpose to check whether the instruments work properly, a preloading test was performed in the first day. The field excavation test was carried out after the sandbags were removed, by excavating the lower part of slope up to about 5 m depth by four steps. In the field test, measuring instruments are set as shown in Fig. 7. The instruments in the slope consisted of numbers of strain gauges on the reinforcements and an inclinometer in the borehole. The stretching invar wires with the dial indicators and the settlement plates were set on the slope to measure displacements of the ground surface. The field measurement was continued on a precise automatic system by using a personal computer.

Results of Field Test

Figs. 10 to 13 show comparison of development of tensile force due to surcharge loading and excavation. Fig. 10 shows the typical measured maximum tensile forces developed in the reinforcements A and C versus the elapsed time. The tensile force developed in the reinforcement reached a stable state immediately after the surcharge loading, and reduced slightly after the loading was removed. Fig. 11 shows the typical measured maximum tensile forces developed in reinforcements A and C versus the elapsed time after excavation. It took about two weeks for the tensile force developed in the reinforcement to reach a stable state under an effect of excavation. This delayed response may be due to the effect of the relic joint in the decomposed granite. When a surcharge loading is applied, the relic joint is compressed immediately and permanently. On the other hand, stress relief produced by excavation may cause the relic joint to expand. Such swelling process is slow, because water absorption needs time for the water to penetrate. The field measurement shows that the swelling process takes about two weeks to reach a stable state.

Figs. 12 and 13 show the measured axial forces developed in the reinforcements for the loading test and the excavation test, respectively. Field measurement shows that the axial forces are not all in tension in case of loading and those are mainly in tension in case of excavation.

Fig. 14 shows the measured horizontal displacement of slope surface for the loading test. Fig. 15 shows those at the borehole location for both loading test and excavation test. Regarding the ground displacement at the borehole location, the ground above the 3.0 m level made a forward movement as the load was increased. However, during excavation, it did not make a noticeable movement, in spite of the fact that a larger axial force was applied to the reinforcement compared with the force applied during loading (see Figs. 12 and 13). It can be assumed that this phenomenon has taken place because a required initial displacement of the natural ground to restrain soils adjacent to reinforcements had already occurred during the loading test.

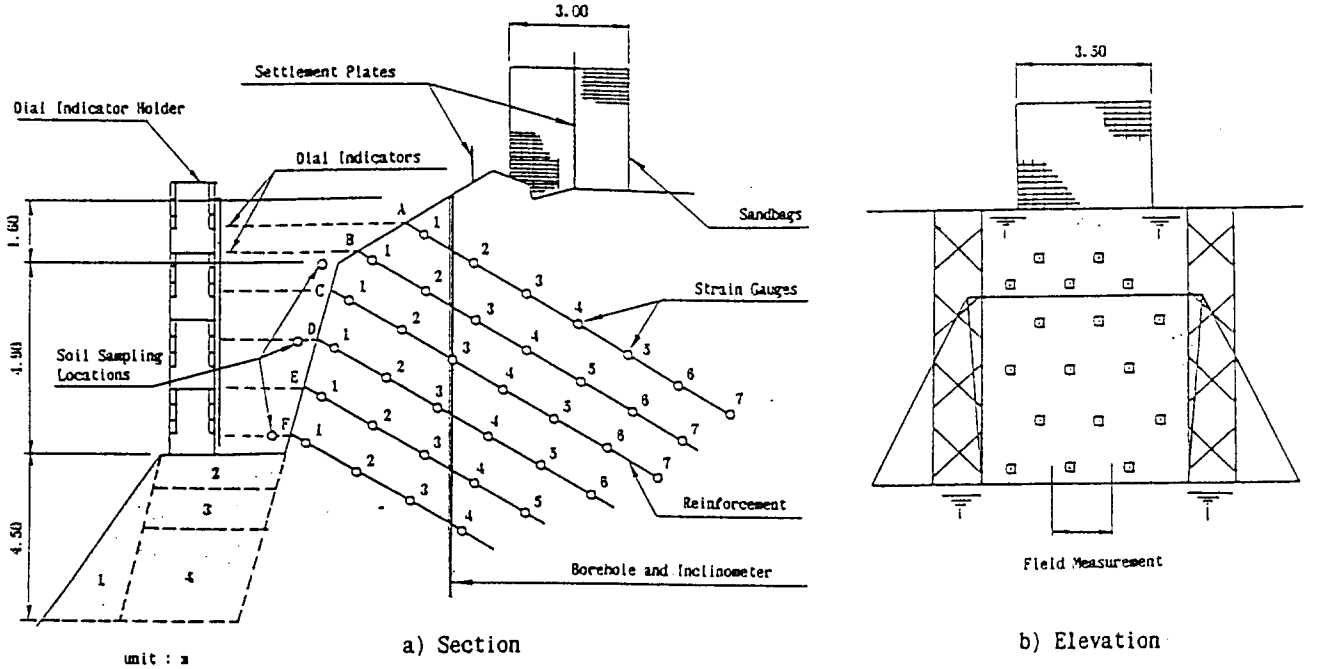

Fig. 7 Section and elevation of reinforced slope for field test at Kashiwara site

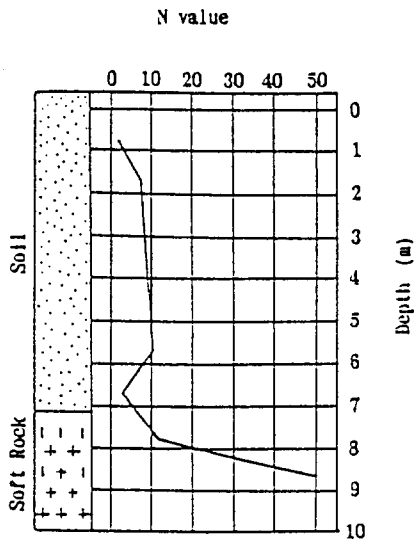

Fig. 8 Soil profile at the borehole location

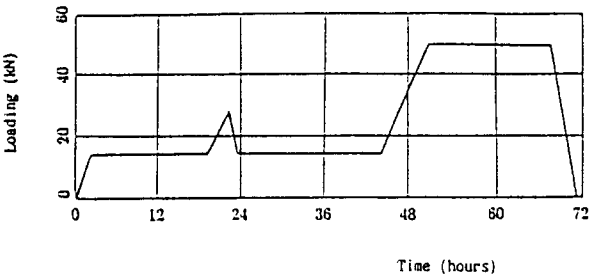

Fig. 9 Applied surcharge load versus time

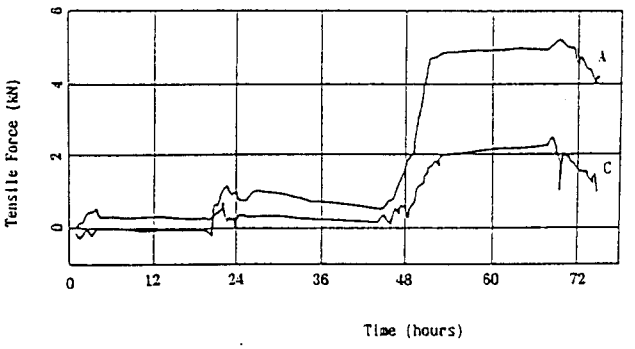

Fig. 10 Measured tensile forces versus time

Test Items	Locations of Sample		
	C	D	E
Unit Weight (kN/m^{-3})	19.7	19.6	19.0
Water Content (%)	8.3	5.7	14.0
Void Ratio	0.55	0.55	0.56
Ignition Loss (%)	3.7	3.5	6.1

Table 1 Test results of decomposed granite

	Depth of Location	
	3.0m	6.0m
Coefficient of Sub-grade Reaction K (MNm^{-3})	46.3	27.3
Modulus of Elasticity E (MPa)	2.817	2.119

Table 2 Result of LLT

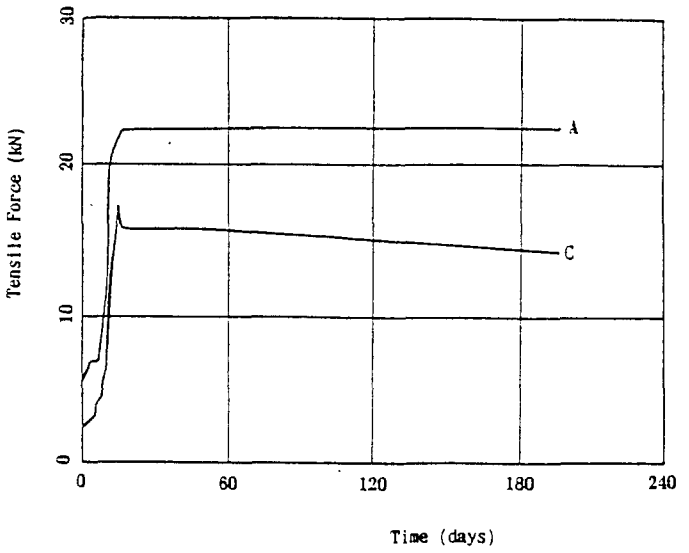

Fig. 11 Measured tensile forces versus time after excavation

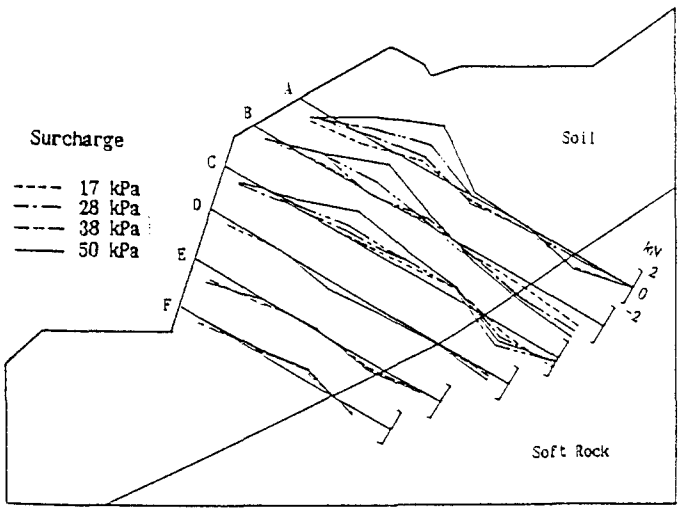

Fig. 12 Measured axial force distribution of reinforcements (loading test)

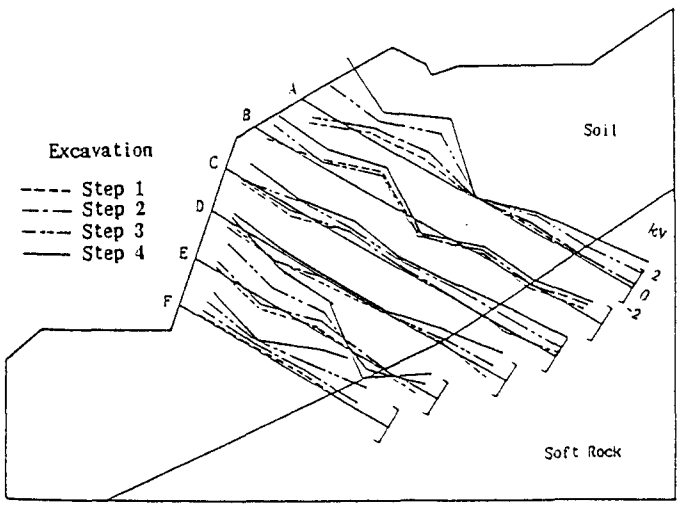

Fig. 13 Measured axial force distribution of reinforcements (excavation test)

Prediction of Test Results and Verification

Finite element analysis was also performed by the hybrid slope stability analysis method (Matsui and San, 1990). The proposed slope stability analysis is a kind of hybrid method of the finite element and limit equilibrium methods. The stress analysis of slope is carried out by means of the finite element method. Based on the stress distribution of the slope, local safety factor surface is constructed. On the other hand, the failure slip surface is determined from the development of the failure shear strain

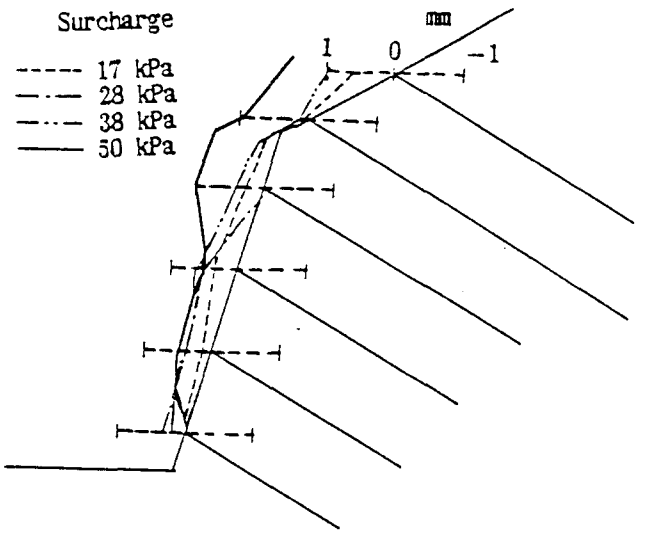

Fig. 14 Measured horizontal displacement of slope surface for loading test

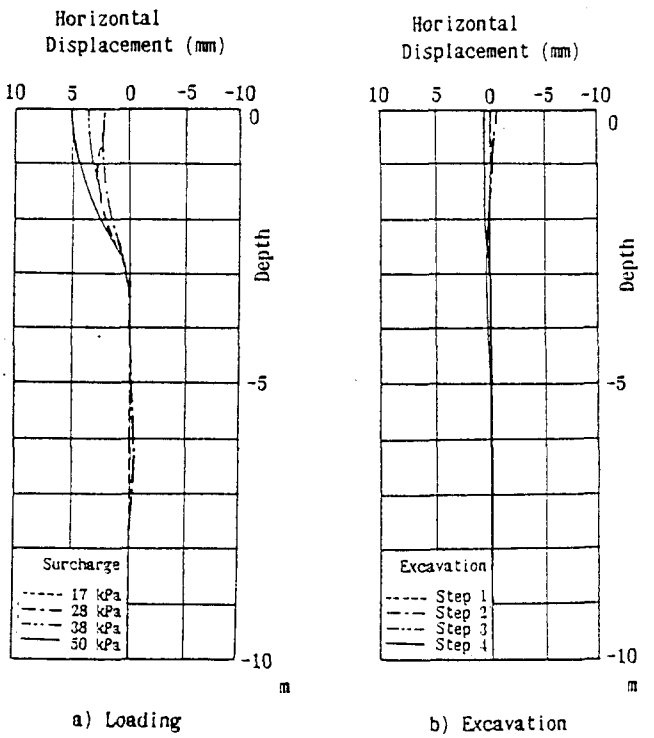

Fig. 15 Measured horizontal displacement at borehole location

zone. Fig. 16 shows the axial force distribution of reinforcements at the stable condition after the completion of the excavation test, obtained from field measurement and finite element analysis. Analytical results approximately agree with the measured ones. The values of the safety factors of the unreinforced slope at the final excavation step obtained by the slice method and the hybrid method are 0.62 and 0.58, respectively (Matsui and San, 1989a). The factors of safety obtained by both methods are close to each ather. However, it is difficult to include the excavation effect on the reinforced slope stability in the slice method. Good agreement between the field data and finite element results demonstrated the validity of the hybrid method to the reinforced cut slope stability analysis.

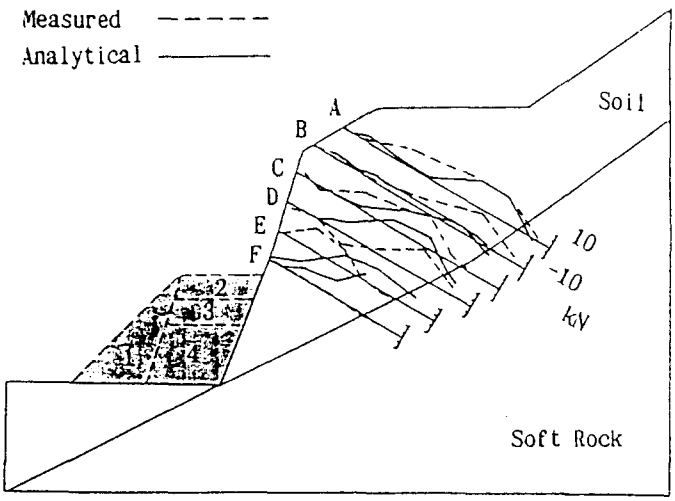

Fig. 16 Measured and analytical axial force distribution of reinforcements after excavation

NOSE CASE – PREDICTION OF CRITICAL EXCAVATION DEPTH

Field Test and Procedure

The second field test was performeed to study the prediction of the critical excavation depth of a reinforced cut slope (Matsui, San and Hayashi, 1990). Fig. 17 shows the section of the reinforced cut slope for the field test. In this site, soil investigation has been performed based on four boring data which include a lateral boring data. The geotechnical section of the site being obtained from the soil investigation is shown in Fig. 18. The slope consists of sandstone, which is hard but cracky. A top layer and D-class sandstone which have the thickness of several meters are completely weathered to residual soils. The elastic wave velocity of residual soils is about 500m/sec. A fracture zone is supposed to exist below the existing retaining wall through soil investigation. As the site is near the mountain top, a ground water level is very deep. Therefore, the slope may not be saturated by the ground water even after hard rain. However, a freezing and thawing impact of the slope surface in winter time may affect the slope stability.

The field test was performed by two stages, as shown in Fig. 17. In the first stage test, the lower part of slope was excavated to the existing road level by two steps. Then, the second stage test was performed by excavating further depth below the existing road level by four steps. The critical excavation depth of the second stage was detemined by Class-A finite element prediction (Matsui and San, 1991). In the field test, measuring instruments were set as shown in Fig. 17. The instruments consisted of numbers of strain gauges on the reinforcements and an inclinometer in the borehole. The field measurement was continued for a long time on a precise automatic system by using a personal computer. The measured data was used to monitor a safety construction of the remedial works. The site observation was continued for about five months in the first stage test and for about three months in the second stage test.

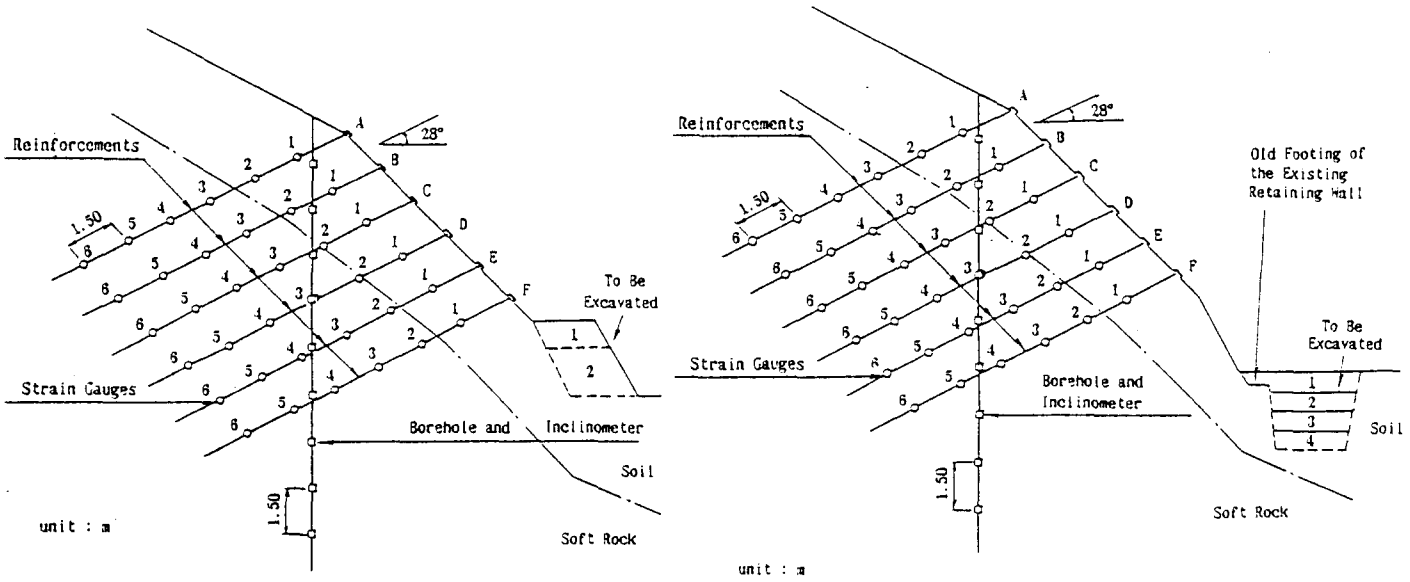

Fig. 17 Section of reinforced slope for field test at Nose site

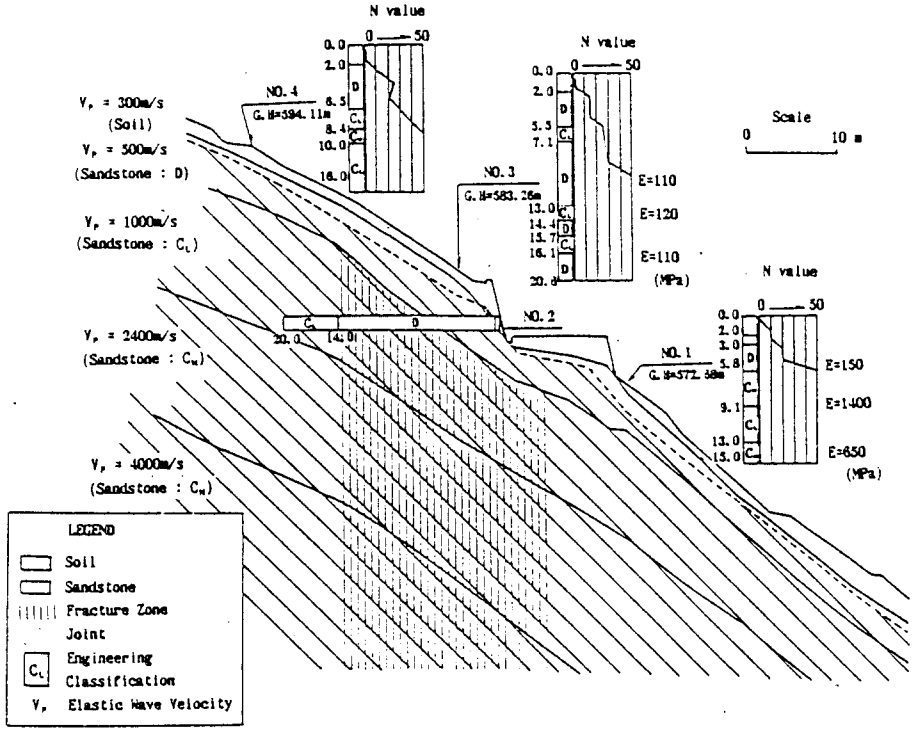

Fig. 18 Geological section of slope

Results of Field Test

Fig. 19 shows the axial force distributions of seven days after the completion of the first step excavation and five months after the completion of the second step excavation in the first stage test. The axial forces developed in the lower three reinforcements are much greater than in the upper three reinforcements. The maximum tensile forces are located around at the interface of the residual soil and the soft rock. Fig. 20 shows the axial force distribution of the reinforcements immediately and three months after the complection of the second stage test. The pattern on the axial force distributions is almost similar to that of the first stage test. The potential failure slip surface probably locates at the interface between the soil and the soft rock.

Fig. 21 shows the long-term variation of the typical measured tensile forces in the reinforcements E and F with the elapsed time. The tensile forces increase after the completion of the first stage excavation and the increasing rate reduces with the elapsed time. Finally, the maximum tensile forces become in stable condition in about 5 months after the excavation. Such creep behavior might be due to the mass relic joints in the weathered residual soil. Also, Fig. 21 shows that the tensile forces of E-2 and F-1 which do not increase signifiantly after the first stage excavation, begin to increase around the second stage excavation. This is supposed to be due to the change of the stress distribution in the slope by the redistribution of stress and the impact of the second stage excavation. As the result, the potential failure slip surface might be changed slightly.

Fig. 22 shows the measured horizontal displacement at the No.4 borehole location. It is seen from this figure that the maximum horizontal displacement is located about five meters below the ground level. It is clear from field measurement that the horizontal displacement is not sensitive to the second excavation impact, because of its small increment.

Prediction of Test Results and Verification

Class-A prediction of the field test by the hybrid slope stability analysis was also performed (Matsui and San, 1991). Fig. 23 shows the axial force distribution of reinforcements at five months after the completion of the first stage excavation obtained from the field measurement and the analysis. Class-A prediction of the critical excavation depth for the second stage excavation was performed. Fig. 24 shows the analytical axial force distribution of reinforcements for different excavation depths. The analytical results show that the maximum tensile force for 2 m depth excavation is about 20 kN. The maximum tensile force of the lowest reinforcement F increases abruptly, when the excavation depth exceeds 2 m. Fig. 25 shows the failure pattern of the reinforced slopes. The failure shear strain of 1 % was assumed in the analysis. The dotted area shown in Fig. 25 represents that the strain exceeds 1 %. The local failure first developes at the toe of the slope and the failure zone extends from the toe to the top of the slope as increasing the excavation depth. Fig. 25 (a) shows the actual slip surface of a minor slope failure in the field test site, which was occurred just before the lower part of slope facing was completed. The failure pattern by the results of the hybrid analysis agrees with the site observation. As the excavation of the second stage test was in danger of the instability of the slope, the determination of the excavation depth had to be given

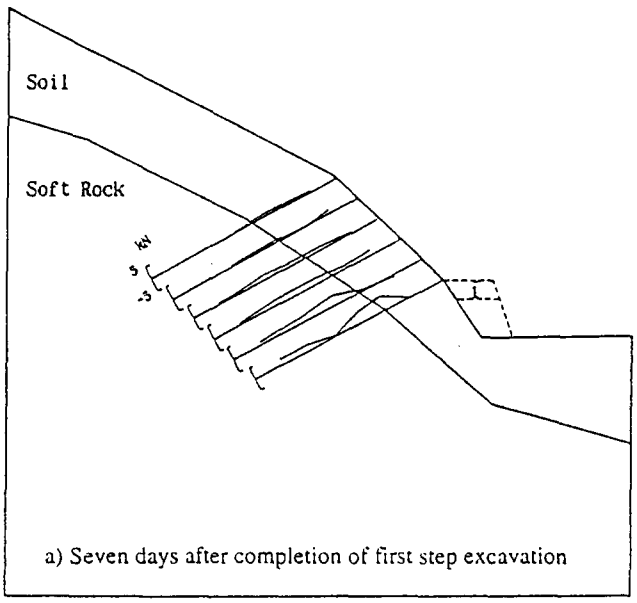

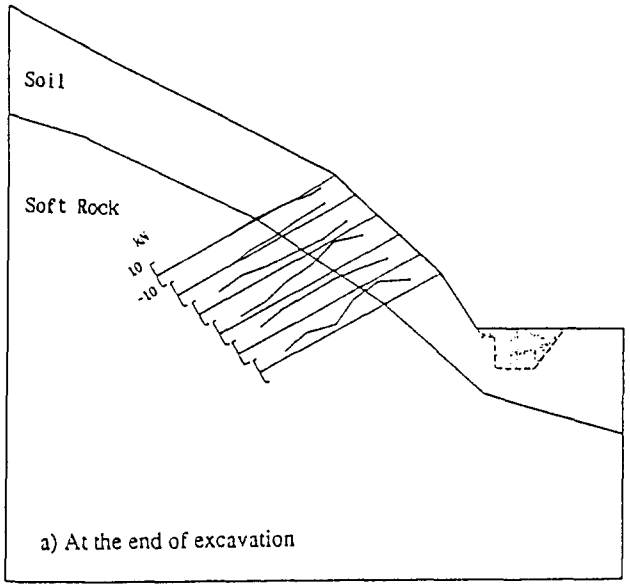

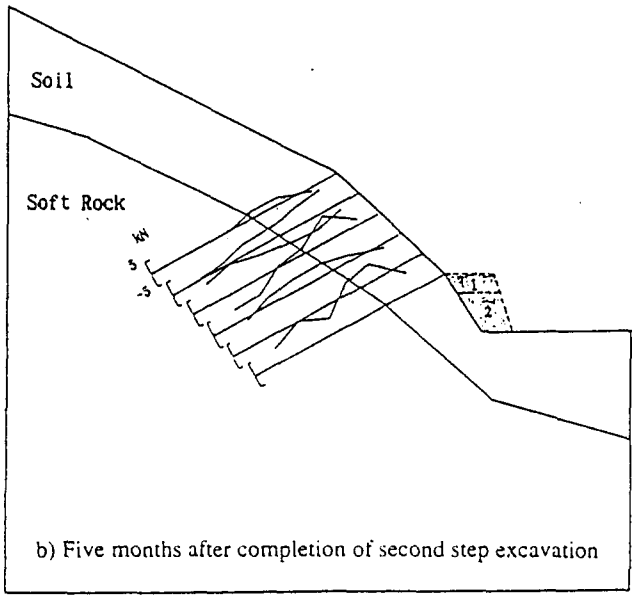

Fig. 19 Measured axial force distribution of reinforcements in first stage field test

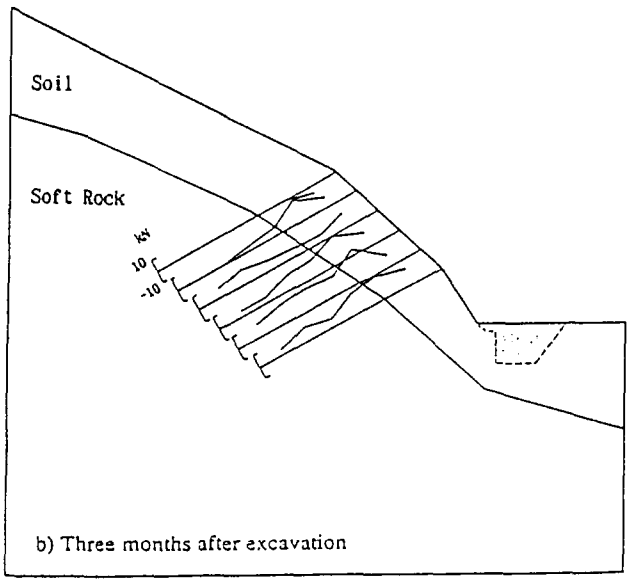

Fig. 20 Measured axial force distribution of reinforcements in second stage field test

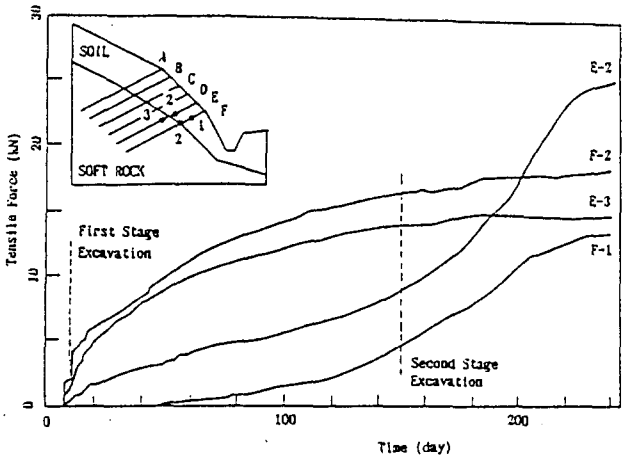

Fig. 21 Long term variation of measured tensile force of reinforcement with elapsed time

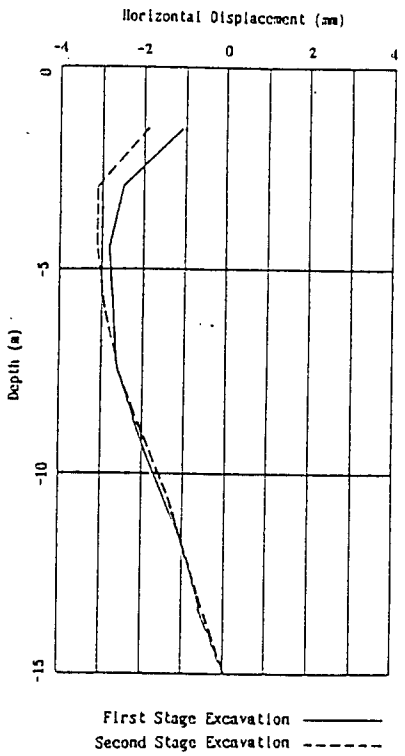

Fig. 22 Measured horizontal displacement at No. 4 borehole location

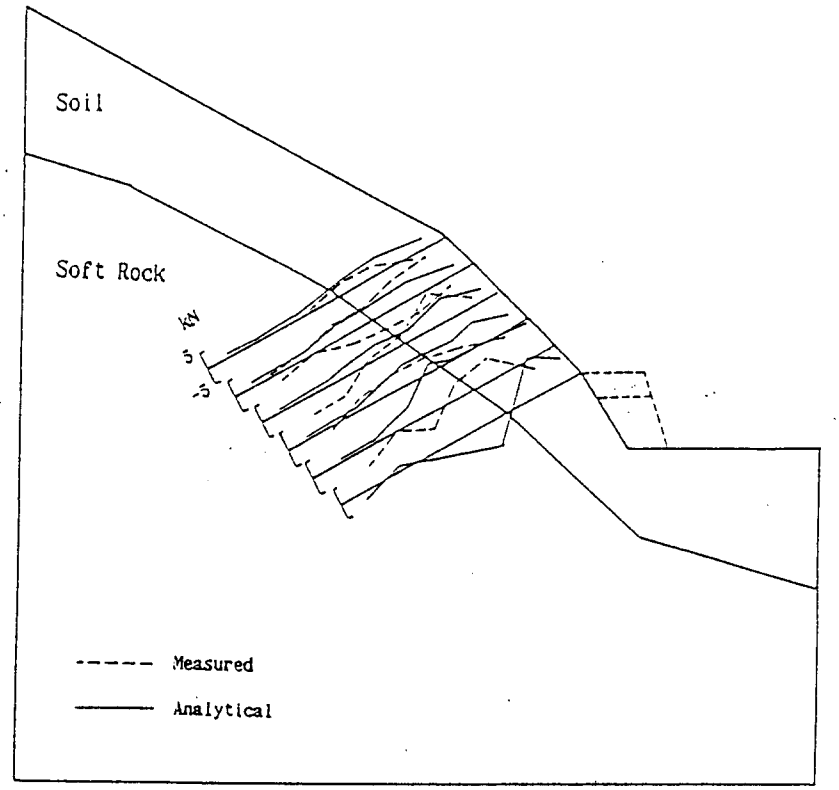

Fig. 23 Measured and analytical axial force distribution of reinforcements at five months after first stage excavation

careful consideration. It was decided that the excavation depth is 2 m based on the Class-A prediction results as described above. Fig. 26 shows the measured and analytical axial force distribution of reinofrcements at the stable condition after the second stage excvation, being obtained from the field measurement and the analysis. The predicted results approximately agreed with the measured one, confirming the availability of the applied hybrid slope stability analysis method.

CLASS-A PREDICTION OF REINFORCED WALL – DENVER WALL

General Remarks

In order to assess the state-of-the-art predictive capability for analysing the performance of geosynthetic-reinforced retaining walls, an International Prediction Symposium of geotextile-reinforced soil retaining wall behavior was held in the University of Colorado at Denver in 1991. Fig. 27 shows the cross-section of the Denver Wall, a geosynthetic-reinforced retaining wall with granular backfill (Wu, 1992). By using the provided laboratory tests results for the triaxial test of the soil, the creep test of the reinforcement and the direct shear test of the interface between soil and reinforcement, Class-A prediction of the performance of the test wall at the end of construction, at 105kPa (15 psi) surcharge as well as the failure loading and failure modes, was performed without any information on the model test results (Matsui and San, 1992). The Class-A prediction by the author's finite element system on the Denver Granular Wall gave its excellent prediction.

Modeling and Parameters Evaluation

As for modeling of granular soil, the generalized plasticity theory (Pastor et al, 1990) is used. Based on the given element test results, the material properties of the granular soil are evaluated and summarized in Table 3. The comparison between the analytical prediction and the test results for granular soil under drained triaxial test condition is shown in Fig. 28. It can be seen from this figure that the agreement betwen the analytical predictiction and the element test results is very good.

As for modeling of interface between granular soil and reinforcement, the effect of the restrained diatancy in the interface between the soil and the reinforcement plays an important role in reinforced soils. Such restrained dilatancy effect causes the change of normal stress on the interface during shearing. Based on Coulomb yield function and its associated flow rule, a restrained dilatancy model for interface between the soil and the structure have been proposed (Matsui and San, 1989b). Based on the given element test results, the material properties of the model of interface between the granular soil and the reinforcement are evaluated and summarized in Table 4. The comparison between the

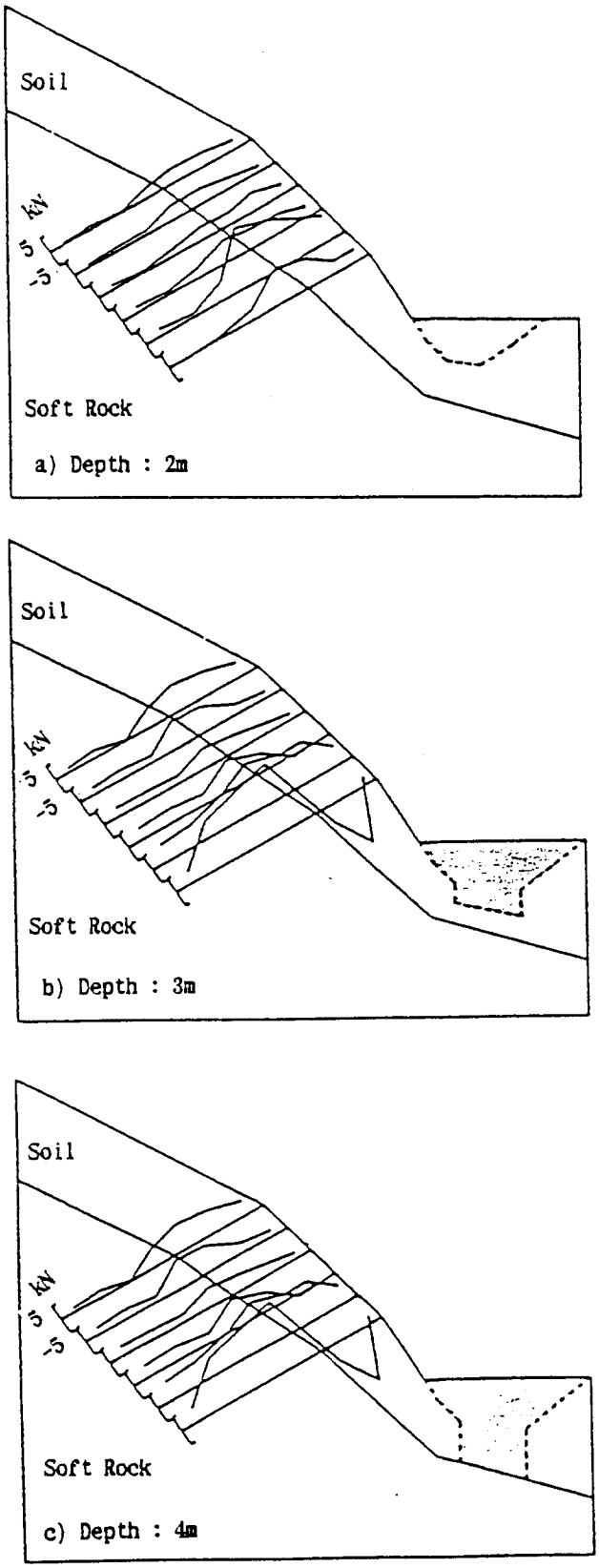

Fig. 24 Analytical axial force distribution of reinforcements for different excavation depths

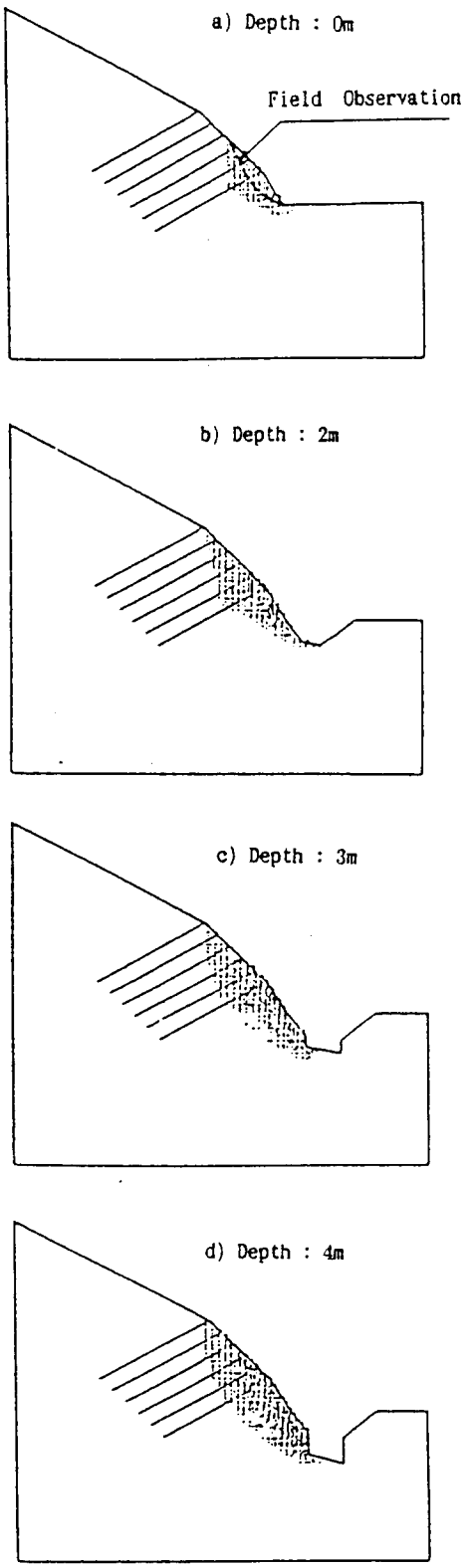

Fig. 25 Failure pattern of reinforced slopes with different excavation depths

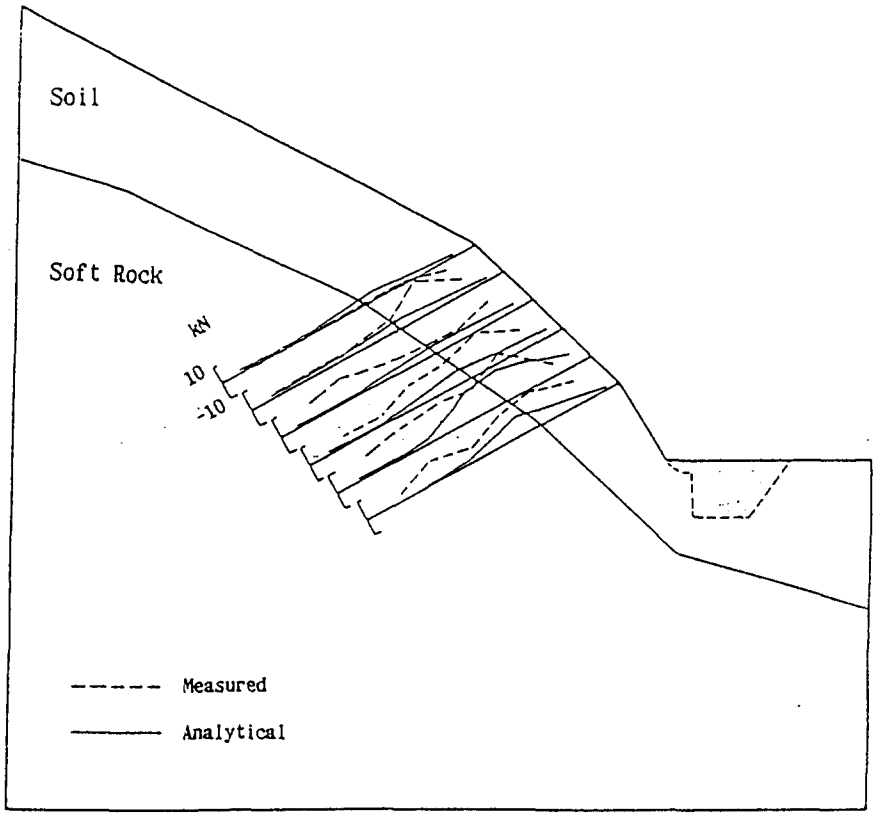

Fig. 26 Measured and analytical force distribution of reinforcements at three months after second excavation

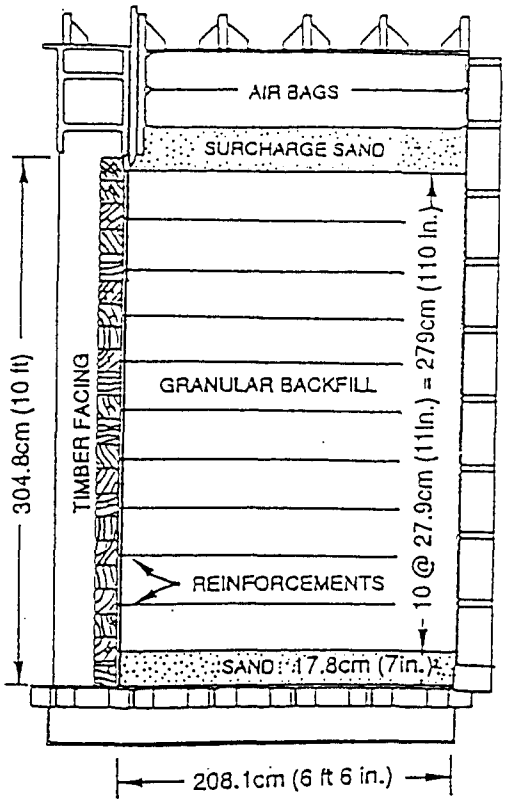

Fig. 27 Cross-section of Denver Wall

analytical prediction and the test results for the interface behavior by direct shear test under constant normal stress is shown in Fig. 29 . It can be seen from this figure that the agreement between the analytical predition and the element test results is very good.

As for modeling of the reinforcement, the creep behavior of the geotextile reinforcement is modeled as visco-elastic material. Kabri (1988) proposed an empirical power function to describe the creep behavior of geotextile. Based on the given element test results, the geotextile material properties are evaluated and summarized in Table 5, in which T and t are in kN-m and hours, respetively. The comparison between the analytical prediction and the creep test results for the reinforcement is shown in Fig. 30. It can be seen from this figure that the agreement between the analytical prediction and the element test results is satisfactory.

Finite Element Analysis

Using material properties obtained form the element test results, as described in the previous section, an finite element analysis of the Denver Wall was conducted. The analysis of the construction of the wall was performed by adding elements from the top of the wall, together with applying the gravity force of each element. The analysis of the loading test was performed by applying pressure to the boundary surface. The creep analysis was performed using initial strain technique.

Table 3 Material properties of granular soil

Elastic bulk modulus K (kN/m²)	37000
Elastic shear modulus G (kN/m²)	43000
Material constant M_g	1.22
Material constant M_f	1.20
Material constant H_o	1800
Material constant α	0.45
Material constant β_o	2.5
Material constant β_1	0.13

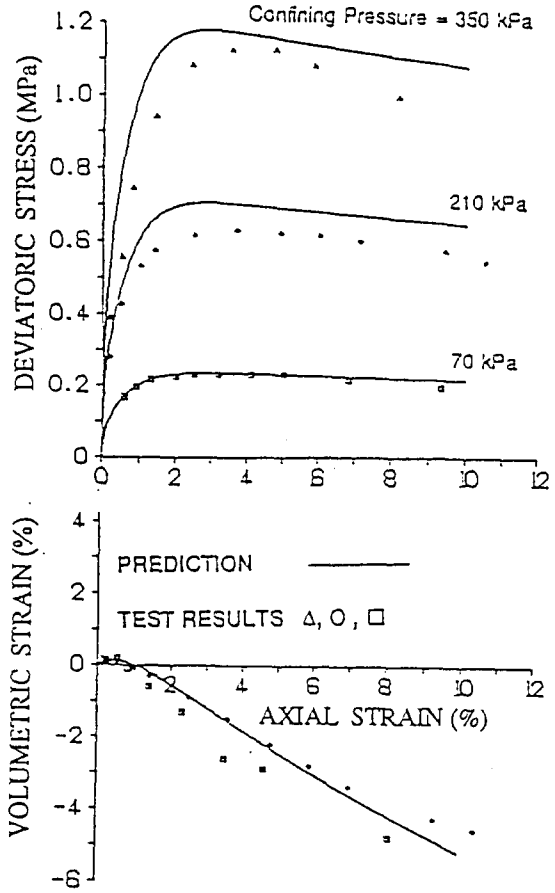

Fig. 28 Comparison between predictions and test results for drained triaxial test

Table 4 Material properties of interface between granular soil and reinforcement

Elastic normal stiffness K_n (kN/m²/m)	37000
Elastic shear stiffness K_s (kN/m²/m)	43000
Material constant M_g	0.40
Material constant M_f	0.35
Material constant H_o(1/m)	1800
Material constant α	0.45
Material constant β_o	2.5
Material constant β_1	0.13

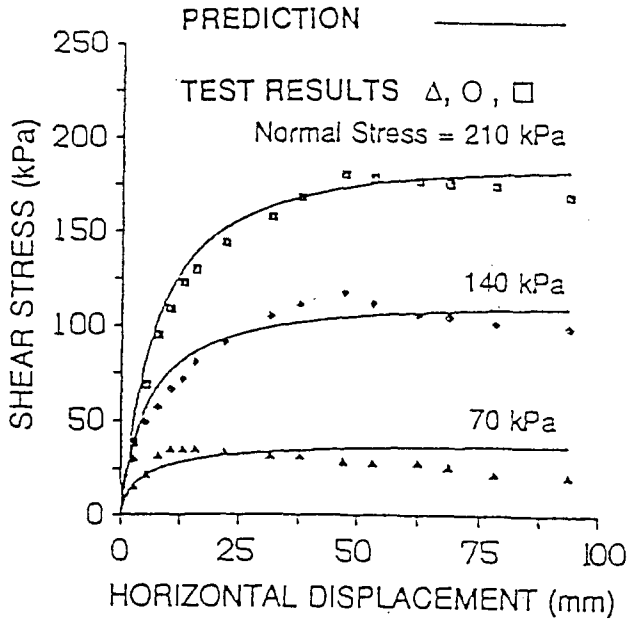

Fig. 29 Comparison between predictions and test results for direct shear test of interface between granular soil and reinforcement

Table 5 Material properties of reinforcement

Material constant ω_o	4.5
Material constant ω_1	25.0
Material constant ω_2	-27.9
Material constant ω_3	849.0
Material constant n	0.171

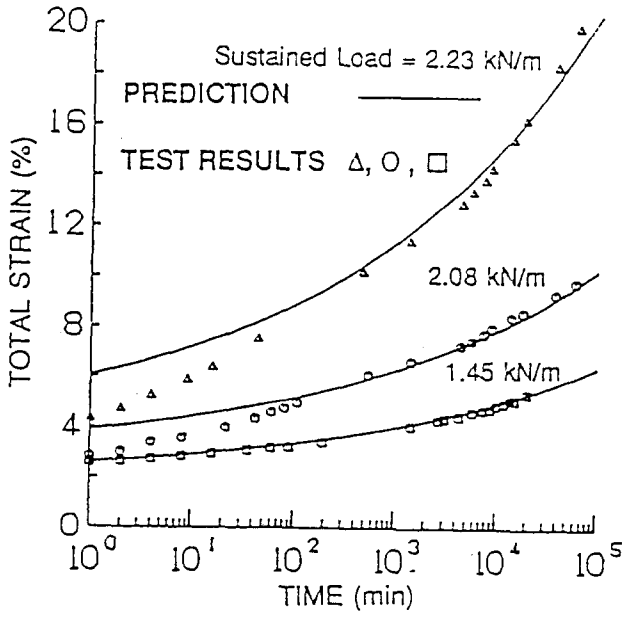

Fig. 30 Comparison between predictions and test results for creep test of reinforcements

Fig. 31 shows the mesh used in the finite element analysis. The solid element used to soil is four node quadrilateral. Joint elements are used between soil and wall facing. Bar elements are used to the reinforcements. Beam elements are used to the wall facing, with EI=7.3x10^{-7} kNm/m, which was obtained from test results of the simple beam test of the facing unit.

Comparison between Test Results and Prediction

Class-A Prediction of Deformation. Comparisons between the test results and predictions of the axial strain distribution in the reinforcements at three different heights 0.15H, 0.52H and 0.88H (measured from the wall base, where H is the total wall height) for the Denver Granular Wall at 105 kPa (15 psi) are shown in Fig. 32. Comparisons between the test results and the predictions of displacement on the top fill surface and the facing movement for the Denver Granular Wall at 105 kPa (15 psi) are shown in Figs. 33 and 34, respectively. From these figures, it can be seen that the agreement between the predictions and the test results is good.

Class-A Prediction of Failure. The failure prediction of the test wall is made by the proposed failure shear strain judgement method (Matsui and San, 1993). The failure of the soil structure is defined as the continuous failure shear zone is fully developed. The value of the shear strain at peak strength

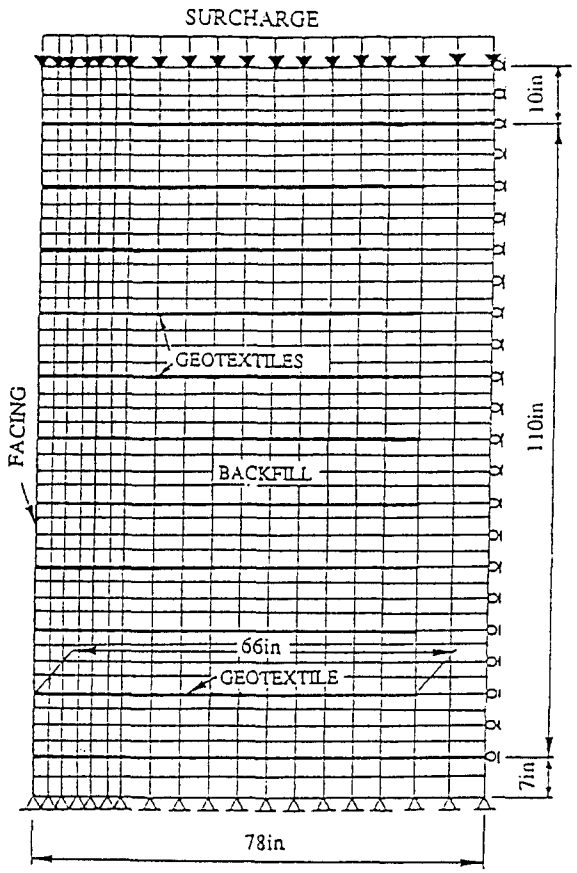

Fig. 31 Mesh used in finite element analysis

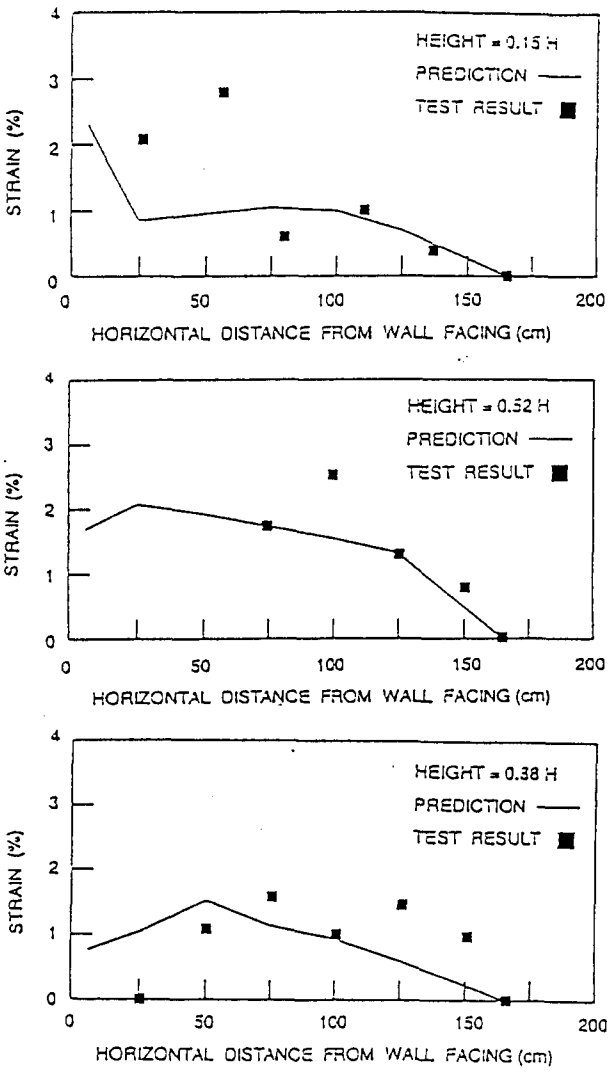

Fig. 32 Axial strain distribution of reinforcement at different heights of Denver Granular Wall at 105 kPa (15 psi)

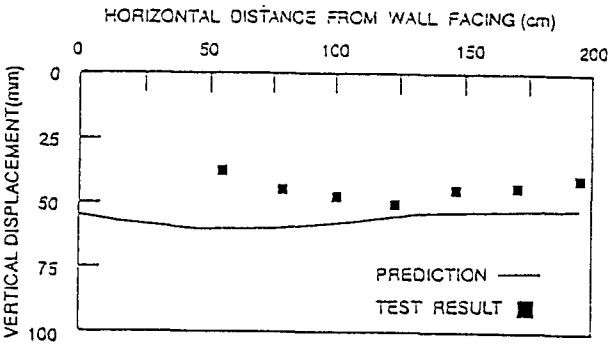

Fig. 33 Comparison between predictions and test results for displacement of top fill surface of Denver Granular Wall at 105 kPa (15 psi)

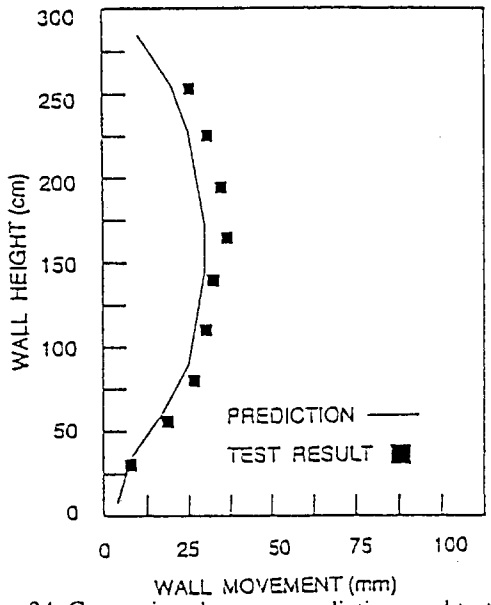

Fig. 34 Comparison between predictions and test results for facing movement of Denver Granular Wall at 105 kPa (15 psi)

appeared in the triaxial test and that at residual strength appeared in the direct shear test are about 5 % and 10 % respectively. The test wall is in plane-strain condition, therefore, 10 % was chosen as the failure shear strain in the prediction. Fig. 35 shows the analytical shear strain contours of the soil of the test wall at different stages. It shows that the predicted failure loading, i.e., the loading when 10 % failure shear strain zone is fully developed, is 203 kPa (29 psi). In the test, surcharge pressure was applied by air bags. A pressure test conducted with the air bag in isolation revealed that the bag can survive up to 350 kPa (50 psi). During loading test of the wall, the air bags burst at 203 kPa (29 psi) surcharge pressure, which was considered as the failure loading. The predicted failure loading of 203 kPa (29 psi) is exactly the same as that obtained in the test.

Fig. 36 shows the analytical load-horizontal displacement curve together with the test data. Note the displacements shown are the maximum horizontal displacement of the facing. The agreement between the analytical results and test data is good. Also it can be seen that the displacement rapidly increases as load exceeds 190 kPa. Therefore, the failure load is expected to be greater than 190 kPa, which is close to the test failure load (203 kPa). Thus, it also demonstrates that failure could be defined as a state of rapidly accelerating displacement. The most noticeable condition of failure may be excessively large displacements. However, it would require experience and judgement to define the point to be monitored and to establish a limit to define failure. On the other hand, the proposed failure shear strain judgement method does not require the specified location to be monitored, though it still needs to establish a limit strain to define failure. In this case history, the failure load would be reduced to 170 kPa and 195 kPa, if 5 % and 8 % failure shear strains are selected, respectively. They are still close to the test failure load (203 kPa).

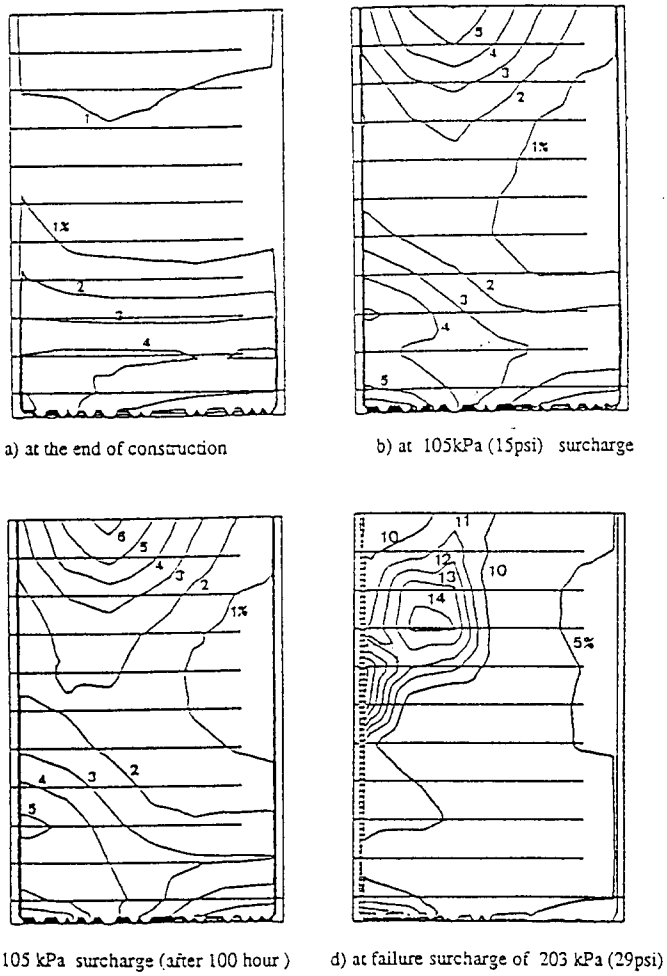

Fig. 35 Analytical shear strain contours of Denver Granular Wall

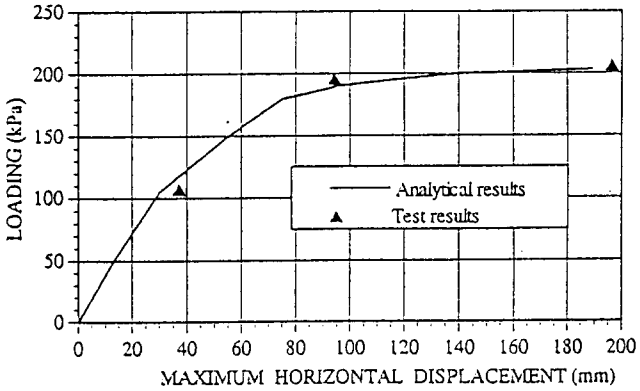

Fig. 36 Relationship between load and horizontal displacement of facing

FEM PREDICTION OF 1G SELF WEIGHT FAILURE TEST ON REINFORED WALL

Outline of Model Test and Procedure

The test wall was a large-scale retaining wall of 6 m height as shown in Fig. 37. The wall was reinforced by 6 layers of principal reinforcements. The reinforcements were 3.5 m long. Each layer was constructed in 1.0 m vertical space. Within every two principal reinforcement layers, an intermediate layer of reinforcement was constructed. The wall was erected with a concrete block facing. The backfill material was compacted every 25 cm lifts.

Measurements in the 1g self weight fialure test on reinforced wall include (1) earth pressure acting on the wall facing, (2) reaction at the wall base, (3) horizontal displacements of the wall facing, (4) horizontal and vertical displacements of top furface, and (5) strain developed on the geotextiles. The locations of the measurement instruments, such as displacement indicators, earth pressure gauges and strain gauges, are also shown in Fig. 37.

The 1g self weight failure test was performed by reducing the length of reinforcements in turns. The cutting of the reinforcements was made by applying heat to the required cutting positions of the reinforcements. The heat was generated by wires that were pre-wound around the required cutting positions of the reinforcements. The sequence of reinforcement cutting is shown in Fig. 38.

Comparison between Test Results and Prediction

The applied procedure of finite element analysis is almost the same as in the previous chapter. Fig. 39 shows the comparison between the test results and analytical sumulation of the horizontal displacement of facing after construction and at failure. The agreement between the test results and analytical simulation of the wall deformation after construction and at

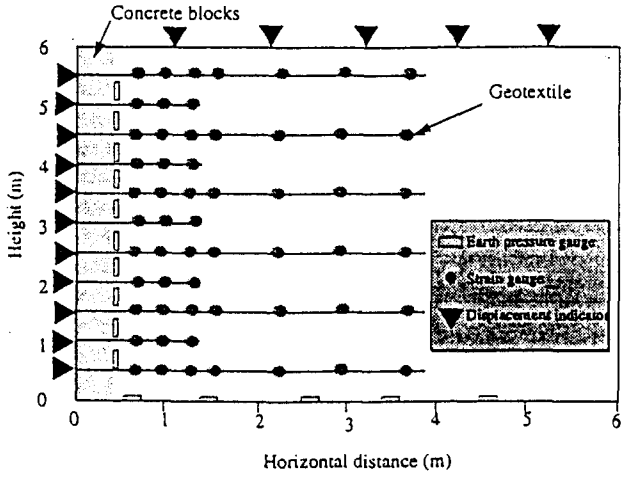

Fig. 37 Large-scale test wall and measuring system

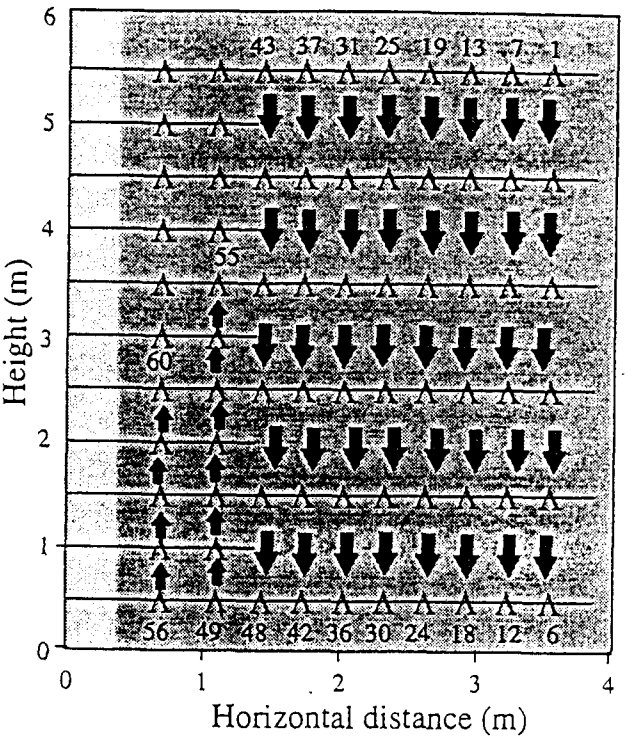

Fig. 38 Sequence of reinforcement cutting

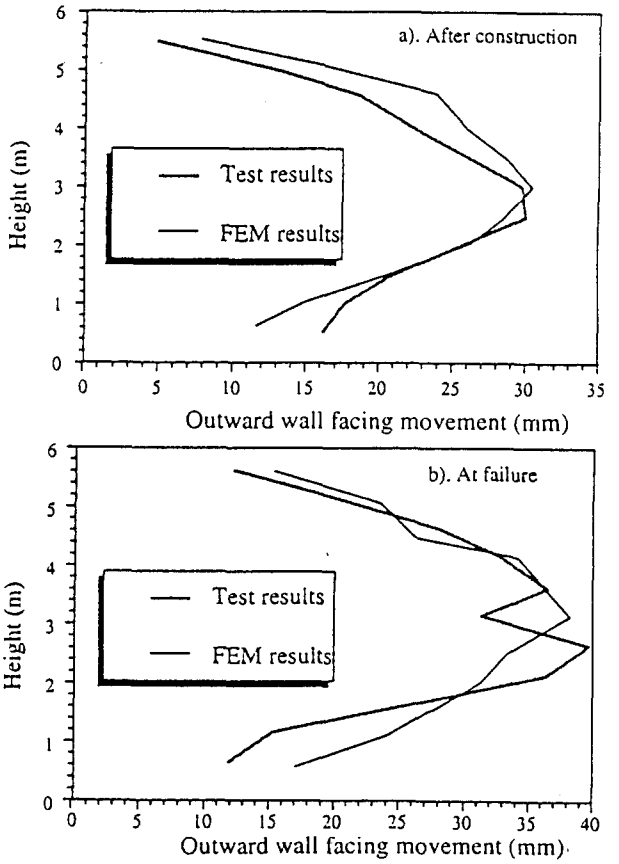

Fig. 39 Comparison between test results and analytical simulation of horizontal displacement of facing

failure is good. The maximum horizontal displacements of the wall at the end of construction and at failure were about 30 mm and 40 mm, respectively. The 30 mm wall movement is a considerable large figure for the 6 m height wall with sandy soil backfill. Such significant wall movement during construction suggests the concrete block facing is quite flexible. An additional 10 mm movement of the wall triggered the failure of wall. The wall failure was a brittle one.

Fig. 40 shows the comparison between the test results and analytical simulation of the strain distribution of the reinforcements after construction. Fig. 41 shows the comparison between the test results and analytical simulation of the strain distribution of the reinforcements at failure. The agreement between the test results and analytical simulation is satisfactory. The maximum strains developed in the reinfrocements at end of construction and at failure were about 1 %.

Fig. 42 shows the comparison between the test results and analytical simulation of the maximum horizontal displacement with various cutting number of the reinforcements. The agreement between the test results and analytical simulation is excellent.

CONCLUSIONS

In this paper, moritoring data and FEM prediction of reinforced cut slopes and retaining walls were described. As the results, some important reinforcement mechanisms were elucidated through measured and analytical results, followed by demonstrating the availability of FEM prediction of reinforced slopes and walls.

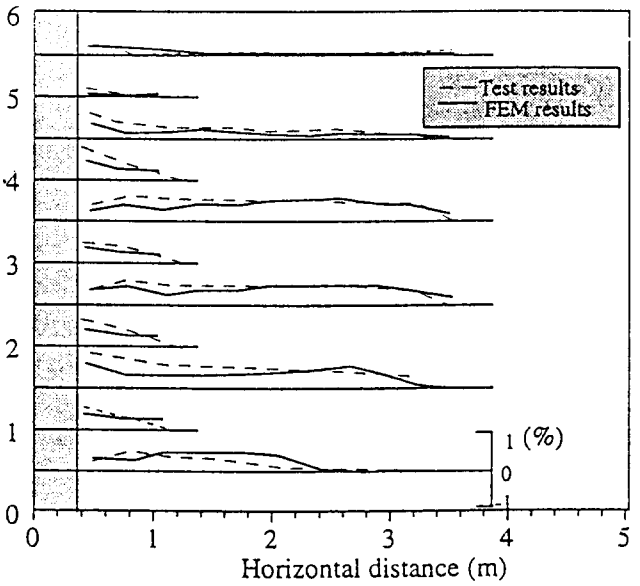

Fig. 40 Comparison between test results and analytical simulation of strain distribution of reinforcements (after construction)

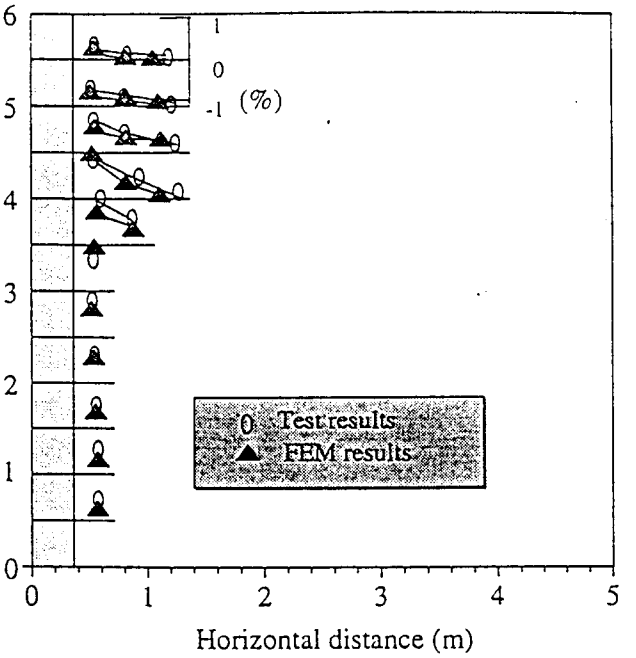

Fig. 41 Comparison between test results and analytical simulation of strain distribution of reinforcements (at failure)

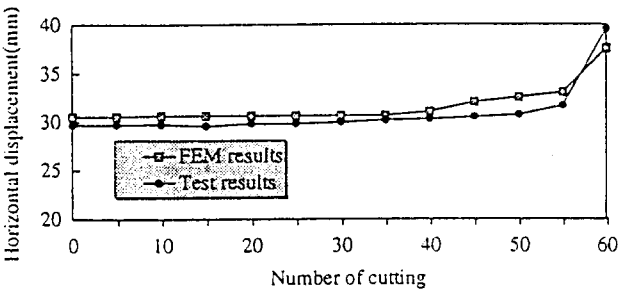

Fig. 42 Comparison between test results and analytical simulation of maximum horizontal displacement with various cutting number of reinforcements

REFERENCES

Kabri, M. H. (1988) : "Creep behaviour of geotextiles", Proc. of International Geotechnical Symposium of Earth Reinforcement, Fukuoka, pp.111-117.

Matsui, T. and San, K. C. (1989 a) : "Verification of the analysis method for reinforced slopes", Proc. 12th Conference on SMFE, Brazil, Vol.2, pp.1277-1279.

Matsui, T. and San, K. C. (1989 b) : "An elastoplastic joint element with its application to reinforced slope cutting", Soils and Foundations, Vol.29, No.3, pp.95-104.

Matsui, T. and San, K. C. (1990) : "A hybrid stability analysis method with its application to reinforced slope cutting", Soils and Foundations, Vol. 30, No.2, pp.79-82

Matsui, T. and San, K. C. (1991) : "Slope stability analysis by shear strength reduction technique", Proc. 7th Conf. on Computer Methods and Advances in Geomechanics, Cairns, Vol.1, pp.499-504.

Matsui, T. and San, K. C. (1992) : "Prediction of two test walls by elasto-plastic finite element analysis", Proc. of Int. Symposium on Geosynthetic Reinforced Soil Retaining Walls, Denver, pp.259-273.

Matsui, T. and San, K. C. (1993) : "Reinforced slope behavior and design methods", Proc. of 1st Tokushima International Seminar, Tokushima, pp.135-160.

Matsui, T., San, K. C., Amono, T. and Otani Y. (1988) : "Field measurement on a slope cutting with tensile inclusions", Proc. 2nd International Conference on Case Histories in Geotechnical Engineering, St. Louis, Vol. 2, pp.1099-1105.

Matsui, T., San, K. C. and Hayashi, K. (1990) : "Design and field test on a reinforced cut slope", Proc. Int. Reinforced Soil Conf., Glasgow, pp.235-239.

Pastor, M., Zienkiewicz, O. C. and Chan, A. H. C., (1990) : "Generalized plasticity and the modeling of soil behavior", International Journal for Numerical Analytical Methods in Geomechanics, Vol. 14, pp.151-190.

Wu, J.H.T. (1992) : "Measured behavior of the Denver Walls", Proc. of Int. Symposium on Geosynthetic-Reinforced Soil Retaining Walls, Denver, pp.31-42.